nature neuroscience

Spike bursts increase amyloid-β 40/42 ratio by inducing a presenilin-1 conformational change

Iftach Dolev[1,4], Hilla Fogel[1,4], Hila Milshtein[1,2], Yevgeny Berdichevsky[1], Noa Lipstein[3], Nils Brose[3], Neta Gazit[1,2] & Inna Slutsky[1,2]

Accumulated genetic evidence suggests that attenuation of the ratio between cerebral amyloid-β Aβ40 and Aβ42 isoforms is central to familial Alzheimer's disease (FAD) pathogenesis. However, FAD mutations account for only 1–2% of Alzheimer's disease cases, leaving the experience-dependent mechanisms regulating Aβ40/42 an enigma. Here we explored regulation of Aβ40/42 ratio by temporal spiking patterns in the rodent hippocampus. Spike bursts boosted Aβ40/42 through a conformational change in presenilin1 (PS1), the catalytic subunit of γ-secretase, and subsequent increase in Aβ40 production. Conversely, single spikes did not alter basal PS1 conformation and Aβ40/42. Burst-induced PS1 conformational shift was mediated by means of Ca^{2+}-dependent synaptic vesicle exocytosis. Presynaptic inhibition *in vitro* and visual deprivation *in vivo* augmented synaptic and Aβ40/42 facilitation by bursts in the hippocampus. Thus, burst probability and transfer properties of synapses represent fundamental features regulating Aβ40/42 by experience and may contribute to the initiation of the common, sporadic Alzheimer's disease.

Changes in conformation and molecular composition of amyloid-β (Aβ) in the brain extracellular space have been proposed to be critical for the development of synaptic and cognitive deficits in Alzheimer's disease[1,2]. Aβ, a normal product of neuronal metabolism[3–5], is produced by sequential limited proteolysis of the amyloid precursor protein (APP) by two aspartyl proteases, β- and γ-secretases[6,7], γ-secretase being the last processing step. Normally, γ-secretase cleavage results in variable 38- to 43-amino-acid Aβ peptides, with Aβ40 and Aβ42 constituting the two most common isoforms. The biophysical and biochemical properties of Aβ vary strongly with its length. Aβ42 aggregates faster[8], although less of it is produced. Small alterations in the molecular composition of Aβ, reflected in the Aβ40/42 ratio, can substantially affect Aβ aggregation kinetics[9,10] and synaptic function[10].

The Aβ40/42 ratio has been suggested to be critical for Alzheimer's disease pathogenesis[11–13]. Genetic studies provide overwhelming evidence that mutations in genes encoding APP or the γ-secretase subunits presenilin 1 (PS1) or presenilin 2 (PS2) are associated with early-onset, autosomal dominant FAD[14]. More than 100 different FAD mutations trigger decline in the Aβ40/42 ratio through relative overproduction of the Aβ42 isoform[15–17] or reduction in Aβ40 production[18], strongly supporting a role of the Aβ40/42 ratio in Alzheimer's disease pathogenesis[19].

Although FAD mouse models have provided valuable insights into Alzheimer's disease pathogenesis, FAD mutations account for only 1–2% of the Alzheimer's disease patient population[20]. Nonetheless, the experience-dependent mechanisms regulating Aβ40/42 changes in the more common, late-onset sporadic Alzheimer's disease remain largely unknown. Elucidating factors that regulate the Aβ40/42 ratio is hence of utmost importance for understanding normal hippocampal function and the transition to the early stages crucial in the pathogenesis of sporadic Alzheimer's disease. To address this question, we explored the physiological regulation of Aβ40 and Aβ42 amounts by activity patterns and synaptic properties in rat hippocampal slices and primary hippocampal cultures. Our data suggest that spike bursts boost Aβ40/42 ratio, by means of a conformational change in the PS1 catalytic subunit of the γ-secretase complex. We explored physiological mechanisms underlying this regulation.

RESULTS

Temporal spiking pattern regulates the Aβ40/42 ratio

It is widely accepted that changes in the external environment are translated in the brain to fluctuations in spike rates. Previous studies have demonstrated that the extracellular concentration of Aβ depends on neuronal and synaptic activity[21–23]. However, it is unknown whether attributes of neuronal activity affect the molecular composition of Aβ. To address this question, we explored the regulation of Aβ42 and Aβ40 species by mean rate versus temporal pattern of spikes (**Fig. 1**). We stimulated rat hippocampal slices for 1 h and then measured the concentrations of Aβ40 and Aβ42 in the artificial cerebrospinal fluid (ACSF) medium ($[Aβ40]_o$ and $[Aβ42]_o$) by sandwich ELISA. As presynaptic terminals have been suggested to be a key site for Aβ production and release[24], we isolated the effect of presynaptic axonal activation on Aβ release by blocking postsynaptic excitatory AMPA and NMDA receptors (AMPARs and NMDARs) with specific antagonists (20 μM DNQX (6,7-dinitroquinoxaline-2,3-dione)

[1]Department of Physiology and Pharmacology, Sackler Faculty of Medicine, Tel Aviv University, Tel Aviv, Israel. [2]Sagol School of Neuroscience, Tel Aviv University, Tel Aviv, Israel. [3]Max Planck Institute for Experimental Medicine, Department of Molecular Neurobiology, Göttingen, Germany. [4]These authors equally contributed to this work. Correspondence should be addressed to I.S. (islutsky@post.tau.ac.il).

Received 26 November 2012; accepted 26 February 2013; published online 7 April 2013; doi:10.1038/nn.3376

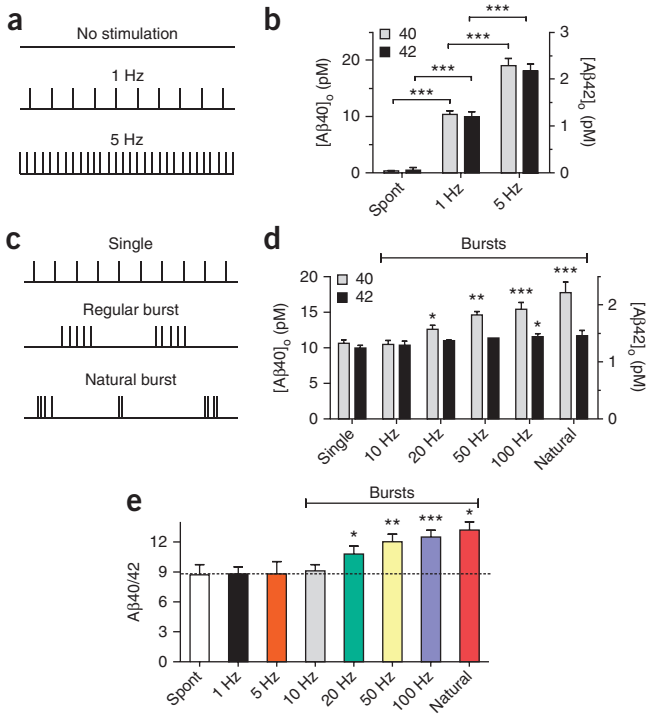

Figure 1 Differential regulation of Aβ40 and Aβ42 isoforms by temporal pattern of afferent input in acute hippocampal slices. (**a**) Stimulation conditions: no stimulation; spikes delivered by field electrodes at 1 Hz; spikes delivered at 5 Hz. The stimulation period was 1 h. (**b**) Increasing stimulation rate from 1 to 5 Hz uniformly increased $[A\beta40]_o$ and $[A\beta42]_o$ (n = 5–7 rats). The fraction of spontaneously released Aβ without stimulation was negligible. (**c**) Stimulation conditions: single spikes at 1 Hz; bursts consisting of five pulses with an inter-spike-interval of 10–100 ms and inter-burst interval of 5 s; 'natural' stimulation pattern[26]. The mean rate was 1 Hz across conditions. (**d**) $[A\beta40]_o$ and $[A\beta42]_o$ measured across stimulation patterns as described in **c**. $[A\beta40]_o$ was higher during 20–100 Hz bursts (n = 4–8 rats) and natural burst discharges (n = 4 rats) as compared to the same number of single spikes (n = 7 rats), whereas $[A\beta42]_o$ did not differ among input patterns ($P > 0.2$). (**e**) Aβ40/42 was similar between periods of spontaneous activity (spont, 4 h, n = 4 rats), 1 Hz (n = 7 rats) and 5 Hz (n = 5 rats) stimulation. Aβ40/42 was 23% higher during 20 Hz bursts (n = 4 rats), 46% higher during 50–100 Hz bursts (n = 4–8 rats) and 50% higher during natural bursts (n = 4 rats). All comparisons are versus single spikes at 1 Hz unless otherwise indicated. $^*P < 0.05$, $^{**}P < 0.01$, $^{***}P < 0.001$ (ANOVA analysis with *post hoc* Bonferroni's multiple comparison tests). Error bars represent s.e.m.

and 50 μM AP5 (D-2-amino-5-phosphonopentanoate), respectively). First, we assessed the effect of the mean rate or total spike number (**Fig. 1a**). The concentrations of spontaneously released Aβ peptides accumulating during 1 h in unstimulated slices were less than 3% of those evoked by 1 Hz stimulation (**Fig. 1b**). A fivefold rise in the stimulation rate (or number of stimuli) resulted in an ~80% increase of both $[A\beta40]_o$ and $[A\beta42]_o$ ($P < 0.001$, **Fig. 1b**). Thus, an increase in the firing rate at a constant frequency upregulated $[A\beta40]_o$ and $[A\beta42]_o$ equally. Consequently, the ratio between $[A\beta40]_o$ and $[A\beta42]_o$ (Aβ40/42) was preserved between periods of stimulation by 1 or 5 Hz and periods of spontaneous activity (measured over 4 h to improve Aβ detection; **Fig. 1e**). Furthermore, a variety of pharmacological manipulations perturbing spontaneous neuronal and synaptic activity in hippocampal cultures had similar effects on $[A\beta40]_o$ and $[A\beta42]_o$ (**Supplementary Fig. 1a**), in agreement with previously reported data[21–23].

Next we assessed the effect of varying the temporal pattern of stimulation on the Aβ40/42 ratio. High-frequency spike bursts have been proposed to be critical for synaptic plasticity, information processing and memory encoding[25]. Thus, we explored their effect on the Aβ40/42 ratio by comparing three stimulation patterns (**Fig. 1c**): (i) single spikes delivered at a constant frequency of 1 Hz; (ii) spike bursts constituting of 5 stimuli at regular frequency of 10, 20, 50 or 100 Hz with 5-s inter-burst-intervals and (iii) a natural pattern that included high-frequency discharges, reproduced from *in vivo* recordings in hippocampal CA1 region of behaving rats as previously described[26]. The mean rate was preserved at 1 Hz for the 1 h duration of stimulation, corresponding to an equal number of stimuli in all protocols. We found that $[A\beta40]_o$ after burst periods increased with the frequency of spikes within the bursts and at frequencies ≥20 Hz was significantly higher than $[A\beta40]_o$ accumulating during periods of single stimuli (**Fig. 1d**). Notably, $[A\beta42]_o$ was less sensitive to the stimulation pattern (**Fig. 1d**). As a result of this isoform-specific behavior, Aβ40/42 was higher after periods of high-frequency bursts than after periods of single spikes (**Fig. 1e**). Increasing the inter-burst interval from 5 to 30 s resulted in a comparable pattern dependency of Aβ40/42 (**Supplementary Fig. 1b**). $[A\beta40]_o$ and $[A\beta42]_o$ were negligible in slices pretreated with inhibitors of β- or γ-secretase and below detection limits in hippocampal slices from $App^{-/-}$ mice (**Supplementary Fig. 1c**,**d**), confirming the specificity of the ELISA.

We obtained similar results in primary hippocampal cultures, which had four times as much $[A\beta40]_o$ and $[A\beta42]_o$ as was present in slice ACSF (**Supplementary Fig. 2a**,**b**), suggesting that the observed Aβ40/42 dynamics was independent of absolute Aβ amounts. Notably, the Aβ40/42 ratio was similar between periods of spontaneous neuronal activity and periods of single spikes in hippocampal cultures as well (**Supplementary Fig. 2c**). We detected no burst-induced changes in the expression of full-length APP, soluble APPα (sAPPα) and the carboxy terminal fragment of APPα (CTFα) as assessed by western blot analysis (**Supplementary Fig. 2d**). Taken together, these results demonstrate that Aβ40/42 is dynamically regulated by bursts owing to higher 'burst sensitivity' of Aβ40 isoform amounts.

Given that postsynaptic site may contribute to the extracellular Aβ pool[27], we explored the involvement of postsynaptic receptor activation in the Aβ40/42 augmentation by bursts. Blockade of NMDA and AMPA receptors in hippocampal slices did not significantly affect $[A\beta40]_o$ and $[A\beta42]_o$ during either single or burst stimulation patterns (**Fig. 2a**,**b**). Additional blockade of metabotropic glutamate receptors 1 and 5 and $GABA_A$ receptors decreased both $[A\beta40]_o$ and $[A\beta42]_o$ by ~25% (**Fig. 2a**,**b**), preserving the Aβ40/42 ratio (**Fig. 2c**). Inhibition of L-type calcium channels by nimodipine caused a ~25% inhibition of $[A\beta40]_o$, but not $[A\beta42]_o$, during either stimulation pattern (**Fig. 2a**,**b**), thereby reducing Aβ40/42 (**Fig. 2c**). However, Aβ40/42 pattern dependency was not affected by any of the applied postsynaptic blockers (**Fig. 2d**). Thus, while both pre- and postsynaptic mechanisms contribute to the extracellular pool of Aβ40 and Aβ42, the Aβ40/42 pattern dependency seems to arise from presynaptic mechanisms.

Spike bursts trigger a PS1 conformational change

Differences in the production, release or degradation of Aβ40 versus Aβ42 peptides could potentially contribute to the observed Aβ40/42 increase by spike bursts. If the relative production of Aβ40 versus Aβ42 is regulated by bursts, the extracellular Aβ40/42 dynamics should reflect the intracellular Aβ40/42 pattern dependency.

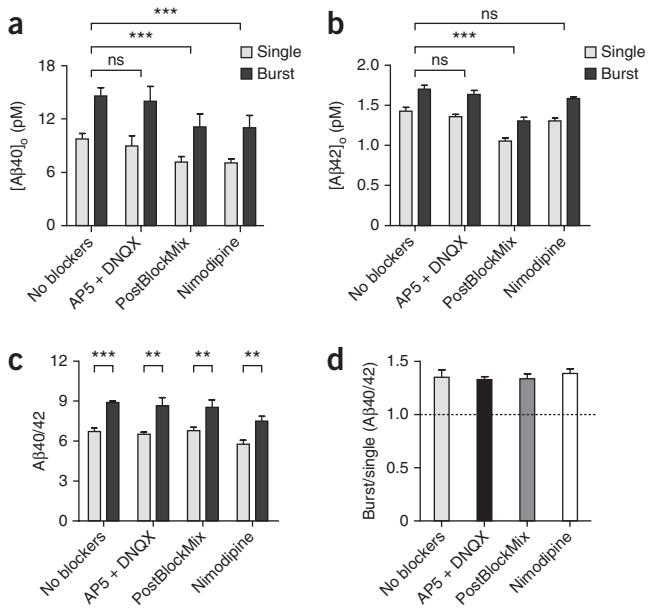

Figure 2 Dependency of Aβ40 and Aβ42 isoforms on postsynaptic activation. (**a**) Effect of postsynaptic blockers on $[Aβ40]_o$ during single and burst stimulation patterns ($n = 4$ rats per group): (i) NMDAR and AMPAR blockers (50 μM AP5 + 20 μM DNQX, respectively), (ii) postsynaptic blocker mix (PostBlockMix): NMDAR + AMPAR + metabotropic glutamate receptor 5 + $GABA_AR$ blockers (50 μM AP5 + 20 μM DNQX + 500 μM MCPG ((*RS*)-α-methyl-4-carboxyphenylglycine) + 30 μM gabazine, respectively), (iii) the L-type VGCC antagonist nimodipine (10 μM). (**b**) Effect of postsynaptic blockers on $[Aβ42]_o$ during single and burst stimulation patterns (tested as in **a**). (**c**) Effect of postsynaptic blockers on Aβ40/42 ratio during single and burst stimulation patterns ($n = 4$ rats). (**d**) Pattern dependency of the Aβ40/42 ratio was not altered by postsynaptic blockers ($n = 4$ rats, $P > 0.3$). $^{**}P < 0.01$, $^{***}P < 0.001$; ns, not significant. ANOVA analysis with *post hoc* Bonferroni's multiple comparison tests (**a**,**b**,**d**), unpaired *t*-test (**c**). Error bars represent s.e.m.

Indeed, bursts caused a ~40% increase in intracellular Aβ40/42 (**Fig. 3a**) owing to an increase in Aβ40 (**Supplementary Fig. 3**). To further explore the mechanism of Aβ40/42 pattern dependency, we assessed the effect of spiking patterns on γ-secretase cleavage. First, we measured $[Aβ40]_o$ and $[Aβ42]_o$ under different stimulation patterns after inhibition of γ-secretase catalytic activity. Application of the γ-secretase inhibitor (GSI) L-685,458 (0.2 μM, 1 h preincubation) reduced absolute Aβ40 and Aβ42 amounts by ~80% (**Fig. 3b**,**c**), suggesting that Aβ production is the main source of Aβ secreted upon stimulation. Notably, GSI completely abolished the burst sensitivity of Aβ40/42 (**Fig. 3d**), indicating that γ-secretase activity contributes to Aβ40/42 augmentation by bursts. Whereas a β-secretase 1 inhibitor (BACE1 inhibitor IV, 0.5 μM, 1 h preincubation) induced reductions in $[Aβ40]_o$ and $[Aβ42]_o$ that were comparable to each other, its effect was uniform between the two stimulation patterns (**Fig. 3b**,**c**), and therefore it did not influence Aβ40/42 pattern dependency (**Fig. 3d**). These results indicate that spike bursts may regulate the relative Aβ40 versus Aβ42 production by means of changes in the γ-secretase cleavage site.

Conformation of PS1 has been suggested to reliably predict relative Aβ40 versus Aβ42 production[28]. To examine whether spike bursts alter Aβ40/42 ratio by modulating PS1 conformation, we monitored PS1 conformation at the level of the single synapse using fluorescence resonance energy transfer (FRET) spectroscopy in live hippocampal neurons. We used a catalytically active FRET reporter of PS1 conformation (proximity of N terminus to loop; see Online Methods and **Fig. 3e**), constructed using a previously described reporter[28], with modified fluorescent proteins: Cerulean (Cer) at the PS1 N terminus and Citrine (Cit) in the large cytosolic-loop domain. The engineered PS1 FRET probe assembles into the γ-secretase complex and is able to reconstitute γ-secretase activity[28]. First, we measured the steady-state FRET efficiency (*E*) using the acceptor photobleaching method at presynaptic boutons expressing Cer-PS1-Cit (**Fig. 3e**). High-magnification confocal images showed an increase in Cer fluorescence after Cit photobleaching (**Fig. 3f**), indicating dequenching of the donor and the presence of FRET at the bouton (**Fig. 3e**). On average, Cer-PS1-Cit FRET efficiency across hippocampal boutons was 0.063 ± 0.005 (mean ± s.e.m.) (**Fig. 3g**), significantly higher ($P < 0.0001$) than the background FRET assessed by photobleaching at 514 nm in neurons expressing PS1 fused only to Cer (0.002 ± 0.008). Next, we verified whether the L166P PS1 FAD mutation, known to increase FRET and lower Aβ40/42 ratio in HEK cells[28], would increase Cer-PS1-Cit FRET in hippocampal synapses. Indeed, L166P increased Cer-PS1-Cit FRET efficiency by 59%, to 0.10 ± 0.008 ($P < 0.001$, **Fig. 3g**), suggesting a FAD-induced shift toward a 'closed' PS1 conformation that corresponds to a lower Aβ40/42 ratio[28,29].

Having confirmed that the Cer-PS1-Cit FRET reporter reflects changes in the Aβ40/42 ratio, we tested whether PS1 FRET depends on spiking patterns. We did not observe FRET changes as function of spiking patterns on a fast timescale of seconds (**Supplementary Fig. 4a**). We then monitored the Cer-PS1-Cit FRET efficiency at a timescale of minutes during 1 h of stimulation, blocking recurrent activity with AMPAR and NMDAR antagonists. Stimulation by single spikes did not alter FRET during the stimulation period (**Fig. 3h**). However, spike bursts induced a reduction in FRET even 5 min after the start of stimulation, reaching a maximum of 60% reduction after 15 min and remaining stable during the rest of the stimulation period (**Fig. 3h**). Burst-induced reduction in FRET was reversible (**Fig. 3i**). Notably, the D257A PS1 point mutation, which blocks PS1 endoproteolysis and γ-secretase activity[30], prevented the effect of bursts on PS1 FRET (*E* was 0.040 ± 0.01 before and 0.043 ± 0.01 after burst stimulation, $n = 15$–17 boutons, $P > 0.6$). Altogether, these results indicate that spike bursts alter PS1 conformation, shifting it toward an open state that corresponds to higher Aβ40 production.

Bursts regulate PS1 conformation through vesicle exocytosis

As synaptic vesicle release has been suggested to directly modulate extracellular Aβ quantity[22,23], we asked whether it mediates changes in PS1 conformation and Aβ40/42 ratio induced by bursts. Therefore, we assessed PS1 conformational changes in neurons lacking synaptic vesicle exocytosis. Tetanus toxin (TeTx), a blocker of SNARE (soluble *N*-ethylmaleimide-sensitive-factor attachment protein receptor)-dependent vesicle exocytosis, abolished the effect of bursts on PS1 conformation (**Fig. 4a**,**b**) and on the intracellular Aβ40/42 (**Supplementary Fig. 3**), suggesting that vesicle exocytosis is required for PS1 conformational changes and increased Aβ40 production induced by bursts. Under TeTx conditions, $[Aβ40]_o$ and $[Aβ42]_o$ were both profoundly decreased (**Fig. 4c**,**d**). We obtained similar results in hippocampal neurons lacking the presynaptic active zone proteins Munc13-1 and Munc13-2 ($Unc13a^{-/-}Unc13b^{-/-}$; **Supplementary Fig. 5**), which have a complete block of glutamate and GABA release[31]. These results indicate that synaptic vesicle exocytosis is also required for secretion of Aβ isoforms.

Given the tight coupling between synaptic vesicle exocytosis and endocytosis, comprising synaptic vesicle recycling at presynaptic

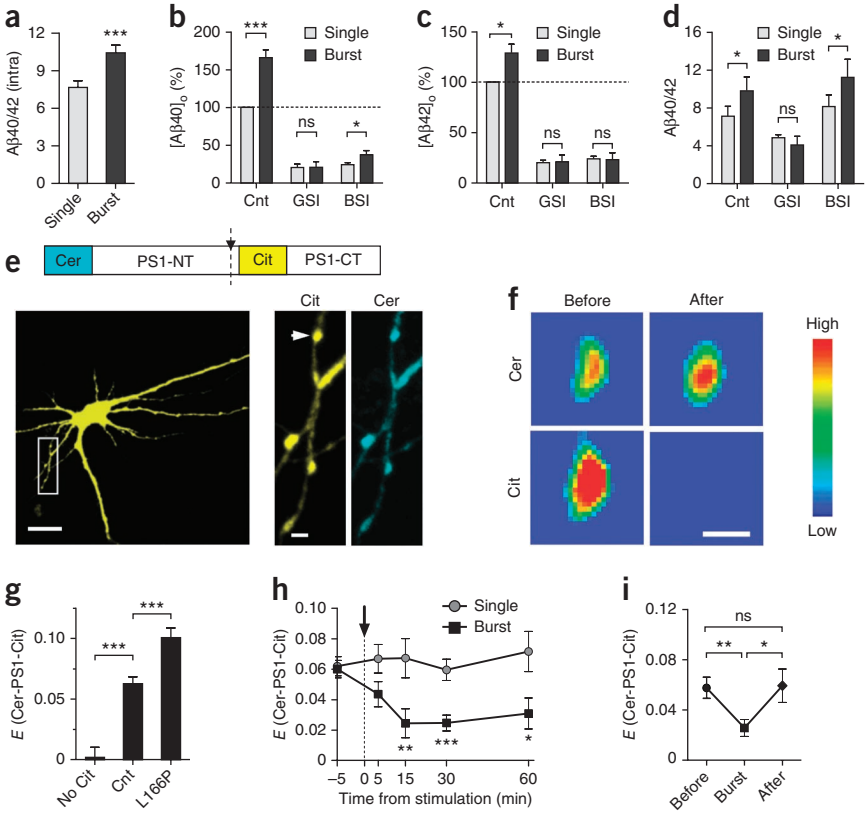

Figure 3 Spike bursts induce PS1 conformational changes in hippocampal neurons. (**a**) Bursts increased the intracellular (intra) Aβ40/42 ratio by a factor of 1.38 ± 0.01 (n = 4 rats). (**b**) Effects of γ-secretase inhibitor (GSI, n = 4 rats) and β-secretase inhibitor (BSI, n = 4 rats) on $[Aβ40]_o$. Cnt, control (standard ACSF). (**c**) Effects of GSI and BSI on $[Aβ42]_o$. (**d**) GSI abolished Aβ40/42 pattern dependency (n = 4 rats, $P > 0.7$), whereas BSI did not affect it (n = 4 rats). (**e**) The Cer-PS1-Cit FRET sensor (top). NT, N-terminal domain; CT, C-terminal. Arrow marks the site of PS1 endoproteolysis. Representative confocal images of a hippocampal neuron expressing Cer-PS1-Cit (bottom). White box in left panel corresponds to the blow-ups in center and right. Arrowhead: the bouton that was bleached for calculation of FRET efficiency (E) in **f**. (**f**) Pseudocolor-coded fluorescence images of Cer-PS1-Cit before and after Cit photobleaching. (**g**) The L166P PS1 mutation increased E (n = 63–114 boutons). The background FRET assessed by photobleaching at 514 nm in neurons expressing PS1 fused only to Cer was negligible (No Cit; n = 20 boutons). (**h**) Time course of burst-induced FRET reduction (n = 26–104 boutons). Single spikes did not induce detectable changes during 60 min of stimulation (n = 36–131 boutons, $P > 0.6$). Arrow marks start of the stimulation. (**i**) Burst-induced E reduction was reversible (n = 38–64 boutons). E was measured before burst stimulation (Before), following 30 min of burst stimulation (Burst) and after 30 min without stimulation (After). Error bars represent s.e.m. Scale bars: 10 μm (**e**, left), 2 μm (**e**, center and right), 1 μm (**f**). $^*P < 0.05$, $^{**}P < 0.01$, $^{***}P < 0.001$; ns, not significant (unpaired t-test).

boutons[32], we explored the role of endocytosis in PS1 pattern dependency. Dynamin-mediated endocytosis has been suggested to regulate extracellular Aβ quantity[23]. Dynasore, a small molecule inhibitor of the dynamin 1 and 2 GTPases, specifically blocks endocytosis triggered by either high- or low-frequency stimulation[33]. Full inhibition of vesicle endocytosis by 80 μM dynasore (ref. 33 and **Supplementary Fig. 4b**) caused a 20% reduction in the inhibitory effect of bursts on Cer-PS1-Cit FRET ($P < 0.05$, **Fig. 4a,b**), but it did not eliminate burst's effects as TeTx did. Although dynasore may inhibit exocytosis through vesicle depletion, this effect is use dependent. Under our experimental

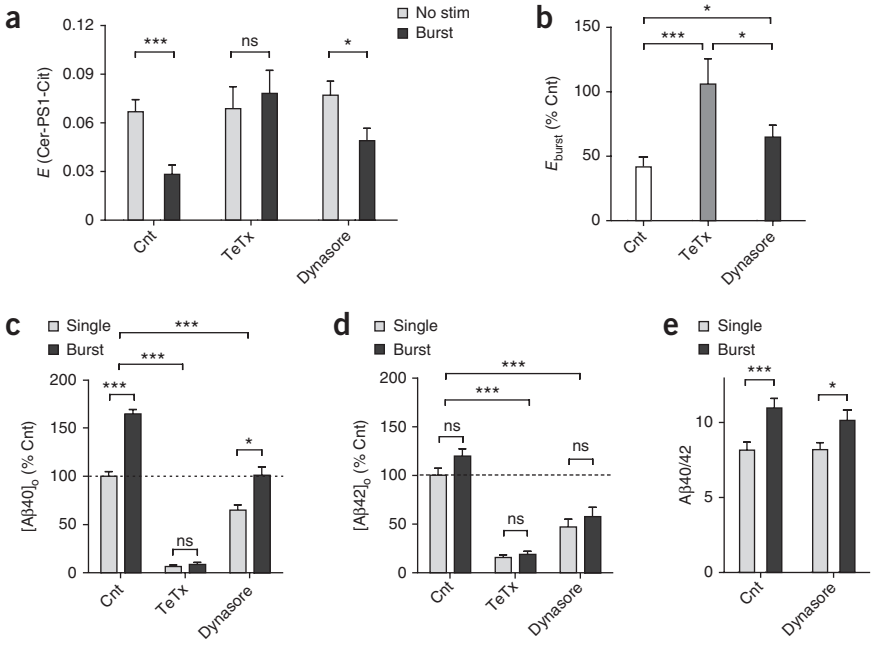

Figure 4 Dependency of PS1 conformation and Aβ40/42 on synaptic vesicle recycling. (**a**) TeTx (33 nM, 37 °C, overnight preincubation) abolished the effect of bursts on FRET efficiency (n = 40–53 boutons, $P > 0.4$) as compared to untreated control (Cnt) cultured neurons (n = 103–113 boutons). Dynasore (80 μM, 15 min) reduced the effect of bursts on FRET (n = 87–93 boutons). (**b**) Summary of the burst-induced effects on E (normalized to the effect of bursts in control) under TeTx and dynasore treatments (same data as in **a**). (**c**–**e**) $[Aβ40]_o$ and $[Aβ42]_o$ measurements in cultured hippocampal neurons. (**c**) Effects of TeTx (n = 7 rats) and dynasore (n = 4 rats) on $[Aβ40]_o$ (as percentage of $[Aβ40]_o$ accumulating under control conditions, single stimulation pattern). (**d**) Effects of TeTx (n = 7 rats) and dynasore (n = 4 rats) on $[Aβ42]_o$ as percentage of $[Aβ40]_o$ accumulating under control conditions (single stimulation pattern). (**e**) Effect of dynasore on the Aβ40/42 dynamics (n = 4 rats). Error bars represent s.e.m. ANOVA analysis with *post hoc* Bonferroni's multiple comparison tests (**b**–**d**) and unpaired t-test (**a**,**e**). $^*P < 0.05$, $^{***}P < 0.001$; ns, not significant.

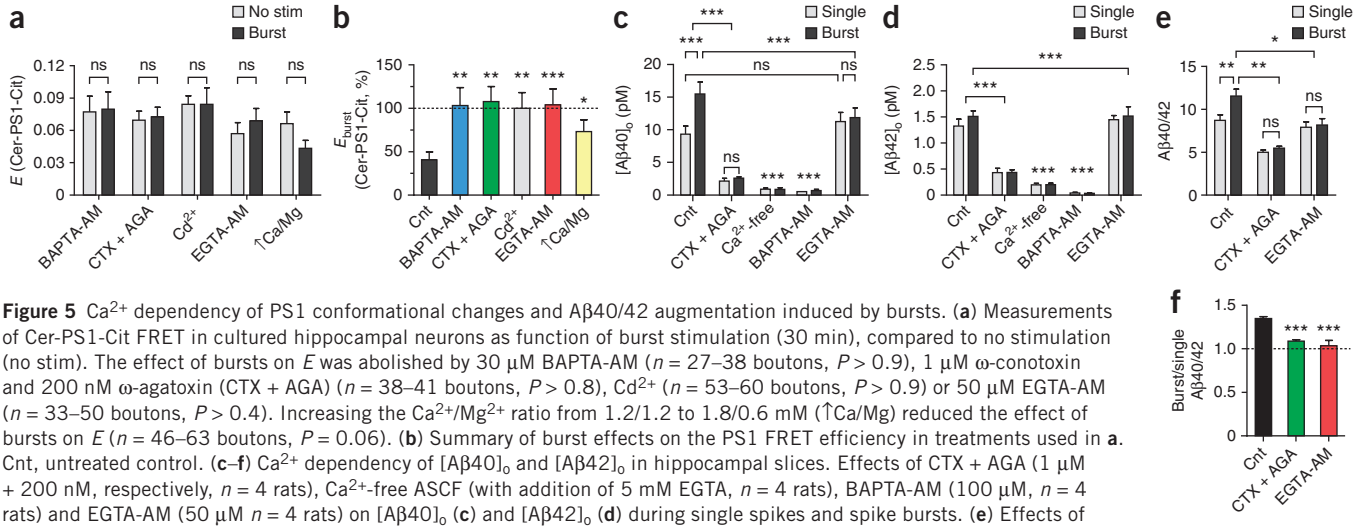

Figure 5 Ca^{2+} dependency of PS1 conformational changes and Aβ40/42 augmentation induced by bursts. (**a**) Measurements of Cer-PS1-Cit FRET in cultured hippocampal neurons as function of burst stimulation (30 min), compared to no stimulation (no stim). The effect of bursts on *E* was abolished by 30 μM BAPTA-AM ($n = 27–38$ boutons, $P > 0.9$), 1 μM ω-conotoxin and 200 nM ω-agatoxin (CTX + AGA) ($n = 38–41$ boutons, $P > 0.8$), Cd^{2+} ($n = 53–60$ boutons, $P > 0.9$) or 50 μM EGTA-AM ($n = 33–50$ boutons, $P > 0.4$). Increasing the Ca^{2+}/Mg^{2+} ratio from 1.2/1.2 to 1.8/0.6 mM (↑Ca/Mg) reduced the effect of bursts on *E* ($n = 46–63$ boutons, $P = 0.06$). (**b**) Summary of burst effects on the PS1 FRET efficiency in treatments used in **a**. Cnt, untreated control. (**c**–**f**) Ca^{2+} dependency of $[Aβ40]_o$ and $[Aβ42]_o$ in hippocampal slices. Effects of CTX + AGA (1 μM + 200 nM, respectively, $n = 4$ rats), Ca^{2+}-free ASCF (with addition of 5 mM EGTA, $n = 4$ rats), BAPTA-AM (100 μM, $n = 4$ rats) and EGTA-AM (50 μM $n = 4$ rats) on $[Aβ40]_o$ (**c**) and $[Aβ42]_o$ (**d**) during single spikes and spike bursts. (**e**) Effects of CTX + AGA and EGTA-AM on Aβ40/42 associated with single and burst patterns ($n = 4$ rats). (**f**) CTX + AGA toxins and EGTA-AM abolished the Aβ40/42 pattern dependency ($n = 4$ rats). "Burst/single" reflects signal detected during burst pattern divided by signal detected during single pattern. Error bars represent s.e.m. $*P < 0.05$, $**P < 0.01$, $***P < 0.001$; ns, not significant. ANOVA analysis with *post hoc* Bonferroni's multiple comparison tests (**b**–**e**) and unpaired *t*-test (**a**,**f**).

conditions (stimulation by bursts consisting of five spikes at 100 Hz, 5 s inter-burst interval), basal synaptic transmission was inhibited by ~60%, whereas synaptic facilitation was not affected (**Supplementary Fig. 4c**). Notably, a tenfold increase in the stimulation rate completely abolished burst-induced PS1 FRET changes in the presence of dynasore (**Supplementary Fig. 4d**). These results indicate that PS1 pattern dependency is not profoundly altered by blocking dynamin-dependent endocytosis in synapses with preserved short-term synaptic plasticity. Although dynasore significantly reduced $[Aβ40]_o$ and $[Aβ42]_o$ (**Fig. 4c**,**d**), the pattern dependency of Aβ40/42 was affected only by 10% (**Fig. 4e**). On the basis of these findings, we conclude that spike bursts induce PS1 conformational changes primarily by means of an increase in synaptic vesicle exocytosis.

Ca^{2+} dependency of PS1 conformational changes

As synaptic vesicle exocytosis during bursts depends on intracellular Ca^{2+} accumulation[34], we explored whether cytosolic Ca^{2+} is the mediator of the PS1 conformational changes induced by bursts.

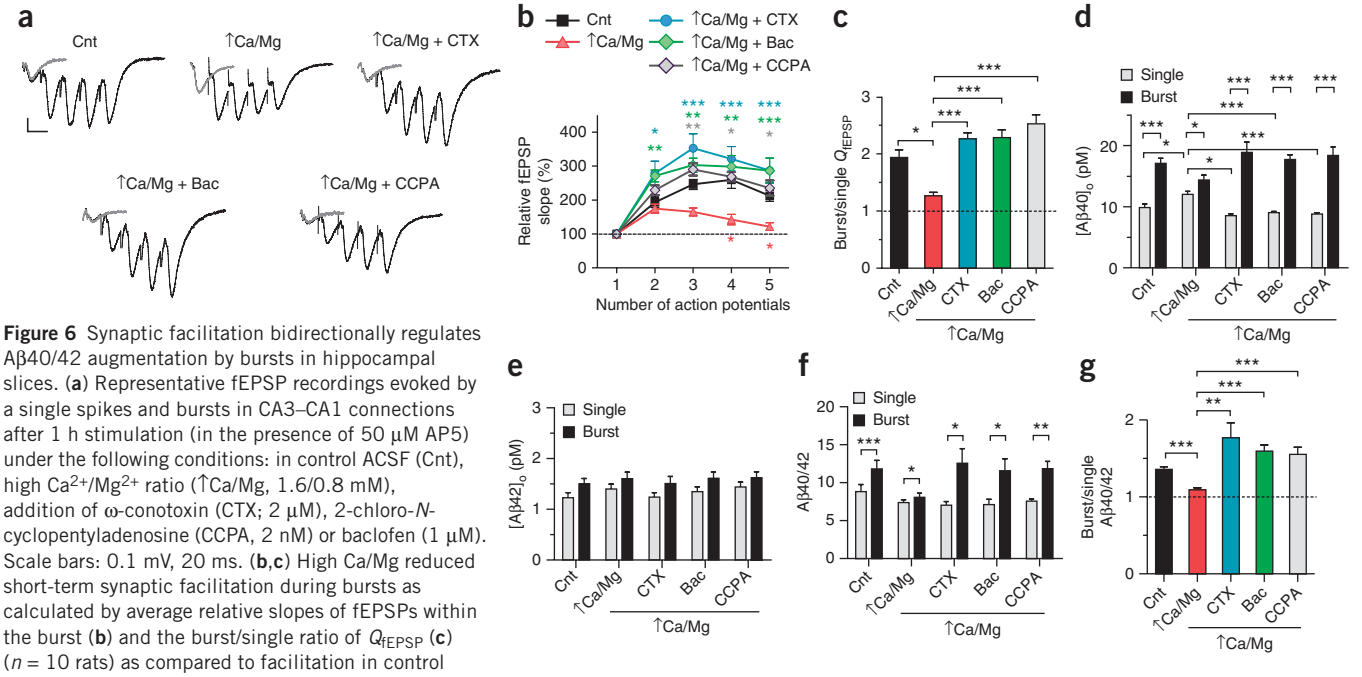

Figure 6 Synaptic facilitation bidirectionally regulates Aβ40/42 augmentation by bursts in hippocampal slices. (**a**) Representative fEPSP recordings evoked by a single spikes and bursts in CA3–CA1 connections after 1 h stimulation (in the presence of 50 μM AP5) under the following conditions: in control ACSF (Cnt), high Ca^{2+}/Mg^{2+} ratio (↑Ca/Mg, 1.6/0.8 mM), addition of ω-conotoxin (CTX; 2 μM), 2-chloro-*N*-cyclopentyladenosine (CCPA, 2 nM) or baclofen (1 μM). Scale bars: 0.1 mV, 20 ms. (**b**,**c**) High Ca/Mg reduced short-term synaptic facilitation during bursts as calculated by average relative slopes of fEPSPs within the burst (**b**) and the burst/single ratio of Q_{fEPSP} (**c**) ($n = 10$ rats) as compared to facilitation in control slices ($n = 8$ rats). CTX ($n = 11$ rats), CCPA ($n = 5$ rats) and baclofen ($n = 9$ rats) rescued short-term facilitation in high Ca/Mg slices. (**d**–**g**) $[Aβ40]_o$ and $[Aβ42]_o$ during single or burst stimulation patterns. (**d**) High Ca/Mg increased $[Aβ40]_o$ during single spikes ($n = 6$ rats), but reduced $[Aβ40]_o$ during spike bursts. CTX, CCPA and baclofen rescued $[Aβ40]_o$ during single spikes ($n = 5$ or 6 rats) and spike bursts ($n = 5$ or 6 rats). (**e**) High Ca/Mg, CTX, CCPA and baclofen did not affect $[Aβ42]_o$ during either stimulation pattern ($n = 5$ or 6 rats, $P > 0.1$). (**f**,**g**) The Aβ40/42 dynamics (**f**) and Aβ40/42 pattern dependency (**g**) under different experimental conditions ($n = 5$ or 6 rats). Error bars represent s.e.m. $*P < 0.05$, $**P < 0.01$, $***P < 0.001$. ANOVA analysis with *post hoc* Bonferroni's multiple comparison tests (**c**–**f**), unpaired *t*-test (**b**,**g**).

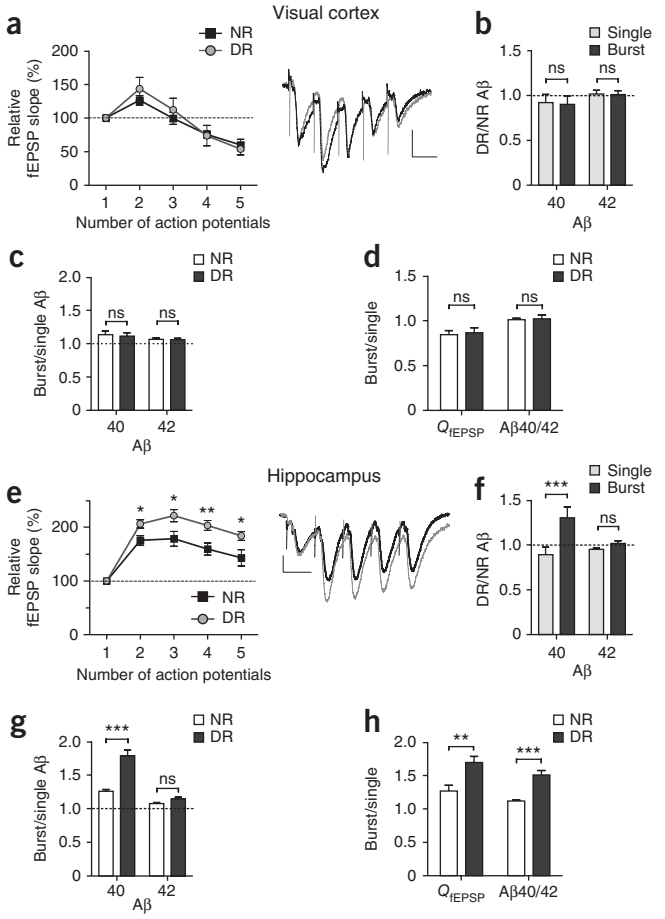

Figure 7 Dark rearing enhances synaptic and Aβ40 facilitation by bursts in CA3–CA1 hippocampal connections. (**a**) Dark rearing did not affect short-term synaptic depression during bursts ($n = 6$ rats, $P > 0.05$) in visual cortex. Right: representative fEPSP recordings evoked by bursts between layer 4 and 2/3 from normally reared (NR) and dark-reared (DR) rats. (**b**) Dark rearing did not affect $[A\beta40]_o$ and $[A\beta42]_o$ at either stimulation pattern ($n = 6$ rats, $P > 0.5$). (**c**) Dark rearing did not affect Aβ40 and Aβ42 pattern dependency in visual cortex ($n = 6$ rats, $P > 0.6$). (**d**) Dark rearing did not affect Q_{fEPSP} ($n = 6$ rats, $P > 0.7$) and Aβ40/42 pattern dependency in visual cortex ($n = 6$ rats, $P > 0.5$). (**e**) Dark rearing increased short-term synaptic facilitation during bursts in CA3–CA1 connections ($n = 8$ rats). Right: representative fEPSP recordings evoked by bursts in hippocampal slices from NR and DR rats. (**f**) Dark rearing increased $[A\beta40]_o$ by 46% during bursts compared with single spikes, whereas it did not affect $[A\beta42]_o$ ($n = 8$ rats). (**g**) Dark rearing enhanced burst/single ratio of Aβ40, but not of Aβ42, in hippocampus ($n = 10$ rats). (**h**) Dark rearing increased the Q_{fEPSP} facilitation ($n = 8$ rats) and Aβ40/42 augmentation by bursts in hippocampus ($n = 8$ rats). Scale bars (**a**,**e**): 0.1 mV, 20 ms. Error bars represent s.e.m. Unpaired *t*-tests. $^*P < 0.05$, $^{**}P < 0.01$, $^{***}P < 0.001$; ns, not significant.

Chelation of intracellular Ca^{2+} by the fast Ca^{2+} buffer BAPTA-AM abolished the effect of bursts on PS1 FRET (**Fig. 5a**,**b**) and intracellular Aβ40/42 (**Supplementary Fig. 3**), implying that the observed changes of PS1 conformation are Ca^{2+} dependent. Notably, chelation of intracellular Ca^{2+} by BAPTA-AM or depletion of extracellular Ca^{2+} ('Ca^{2+}-free condition') reduced both $[A\beta40]_o$ and $[A\beta42]_o$ by >90% (**Fig. 5c**,**d**), indicating that Ca^{2+} is required for secretion of Aβ isoforms.

As voltage-gated calcium channels (VGCCs) are key for synaptic vesicle exocytosis, we examined how blockade of presynaptic VGCCs affects PS1 conformational changes induced by bursts. Application of 1 μM ω-conotoxin and 200 nM ω-agatoxin, specific blockers of N- and P/Q-type VGCCs, respectively, completely abolished the effect of bursts on PS1 FRET (**Fig. 5a**,**b**), suggesting that Ca^{2+} flux through the presynaptic VGCCs is required for the pattern-dependent regulation of PS1 conformation. These PS1 structural changes were accompanied by a profound reduction in absolute $[A\beta40]_o$ and $[A\beta42]_o$ (**Fig. 5c**,**d**) and the Aβ40/42 pattern dependency (**Fig. 5e**,**f**). Moreover, cadmium, a nonspecific VGCC blocker, prevented reduction in Cer-PS1-Cit FRET by bursts as well (**Fig. 5a**,**b**).

Next, we tested whether PS1 conformation and Aβ40/Aβ42 depend on presynaptic Ca^{2+} accumulation during high-frequency spike bursts. We used the slow Ca^{2+} buffer EGTA, which can effectively chelate 'residual' Ca^{2+}, thus preventing synaptic facilitation during bursts. Application of the membrane-permeant EGTA-AM at low concentration (50 μM) indeed reduced by 70% synaptic facilitation of excitatory postsynaptic currents (EPSCs) measured by voltage-clamp whole-cell recordings (**Supplementary Fig. 6**), whereas it reduced EPSCs evoked by single spikes by only 20% ($n = 9$ rats, $P < 0.05$). Notably, EGTA-AM abolished PS1 FRET changes (**Fig. 5a**,**b**) and Aβ40/42 augmentation (**Fig. 5e**,**f**) induced by bursts. EGTA-AM impaired Aβ40/42 burst sensitivity by means of reduction in $[A\beta40]_o$ during bursts and without altering $[A\beta40]_o$ and $[A\beta42]_o$ during single spikes (**Fig. 5c**,**d**). Together, these results imply that burst-induced accumulation of the intracellular Ca^{2+} entering through presynaptic VGCCs triggers a PS1 conformational change, resulting in Aβ40/42 augmentation.

Bidirectional regulation of Aβ40/42 by synaptic dynamics

As bursts induced changes in PS1 conformation and Aβ40/42 by means of Ca^{2+}-mediated synaptic vesicle exocytosis and depended on residual Ca^{2+} required for synaptic facilitation[34], we asked whether Aβ40/42 augmentation can be regulated by the mechanisms tuning short-term synaptic facilitation. To address this question, we pharmacologically manipulated basal neurotransmitter release, which is known to inversely correlate with short-term synaptic plasticity[35]. First, we enhanced release probability by increasing the Ca^{2+}/Mg^{2+} ratio (high Ca/Mg) in the ACSF from 1.2/1.2 to 1.6/0.8 mM and subjected slices to 1 h stimulations by single spikes or spike bursts. Extracellularly recorded field excitatory postsynaptic potentials (fEPSPs) evoked by spike bursts were used to assess short-term synaptic plasticity in connections between the CA3 and CA1 subregions of the hippocampus. As expected, high Ca/Mg resulted in attenuation of synaptic facilitation (**Fig. 6a**,**b**), indicating an increase in basal neurotransmission. We also calculated the mean charge transfer per action potential (Q_{fEPSP}) by dividing the integral under the fEPSP curve by the number of spikes. Given the decreased facilitation, the ratio between Q_{fEPSP} during the burst stimulation pattern and the single-spike pattern was significantly reduced by high Ca/Mg (**Fig. 6c**). Overall synaptic strength under these conditions, evaluated by the slope of the input/output relationship, was ~45% greater than in standard ACSF (**Supplementary Fig. 7a**). The dynamics of Aβ40/42 followed the change in synaptic release properties, showing lower Aβ40/42 during bursts as a result of reduction in $[A\beta40]_o$ burst sensitivity (**Fig. 6d–g**). The decrease in synaptic facilitation by high Ca/Mg resulted in diminished PS1 conformational changes induced by bursts (**Fig. 5a**,**b**).

To test whether these changes in Aβ40/42 are reversible and can be regulated in the opposite direction, we increased synaptic facilitation by reducing basal neurotransmitter release in slices incubated in high Ca/Mg by (i) blocking presynaptic N-type VGCCs by ω-conotoxin

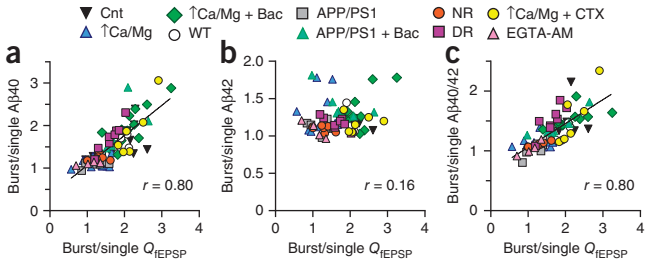

Figure 8 Correlation between short-term plasticity in CA3–CA1 synaptic connections and dynamics of Aβ isoforms per individual animal across different experimental conditions. (**a**) Pooled data ($n = 70$ animals) showing positive correlation between Q_{fEPSP} and Aβ40 dynamics (slope of linear fit, 0.84 ± 0.05; Spearman $r = 0.80$, $^{***}P < 0.0001$). Cnt, control; WT, wild-type; Bac, baclofen; CTX, ω-conotoxin; NR, normally reared; DR, dark reared. (**b**) No correlation was found between Q_{fEPSP} and Aβ42 dynamics (Spearman $r = 0.16$, $n = 70$ animals, $P > 0.05$). (**c**) Q_{fEPSP} facilitation positively correlated with Aβ40/42 dynamics (slope of linear fit, 0.40 ± 0.04; Spearman $r = 0.80$, $n = 70$ animals, $^{***}P < 0.0001$).

GVIA (2 μM); (ii) activating presynaptic adenosine-1 receptors (A_1Rs) with the agonist CCPA (2-chloro-*N*-cyclopentyladenosine; 2 nM); or (iii) activating $GABA_B$ receptors by baclofen (1 μM). All these pharmacological manipulations rescued basal synaptic transmission (**Supplementary Fig. 7a**), with a consequent increase in synaptic facilitation (**Fig. 6a–c**). We obtained similar results using whole-cell voltage-clamp recordings (**Supplementary Fig. 7b–d**). These reverse changes in synaptic release properties were paralleled by changes in Aβ40/42. Increase in synaptic facilitation boosted $[Aβ40]_o$ burst sensitivity and, therefore, Aβ40/42 during periods of high-frequency firing (**Fig. 6d–g**), implying bidirectional regulation of Aβ40/42 by synaptic release properties.

Finally, we established the relationship between synaptic release properties and Aβ40/42 dynamics during spike bursts in the APPswe/PS1dE9 (APP/PS1) transgenic mouse FAD model that shows reduced Aβ40/42 (ref. 36). Mice were examined at the early stage (3 months), before the appearance of amyloid plaques[36]. Short-term facilitation in CA3–CA1 connections of APP/PS1 mice was significantly lower ($P < 0.01$) than in wild-type mice (**Supplementary Fig. 8a–c**), indicating higher glutamate release probability. In parallel to the reduced synaptic facilitation, the Aβ40/42 ratio in APP/PS1 hippocampi lost its sensitivity to bursts (**Supplementary Fig. 8d–g**). Increasing presynaptic inhibition by baclofen rescued synaptic facilitation in APP/PS1 CA3–CA1 connections and restored the burst sensitivity of Aβ40/42 (**Supplementary Fig. 8**). Thus, APP/PS1 FAD mutations, in addition to constitutively reducing the Aβ40/42 ratio, lower Aβ40/42 dynamic range during burst inputs. Of note, we obtained similar results using ELISAs from two other manufacturers for human Aβ40 and Aβ42 (**Supplementary Fig. 9**), verifying the reliability of the data obtained.

Sensory experience regulates synaptic and Aβ40/42 dynamics

We tested the biological relevance of Aβ40/42 physiological dynamics by exploring whether it can be regulated by *in vivo* elicited, experience-dependent synaptic modifications. Neuronal circuits in the primary sensory cortices are shaped by sensory experience during critical periods in early postnatal life[37]. Information about sensory stimuli originating from primary visual cortex (V1) is forwarded to the hippocampus through the perirhinal and entorhinal cortices[38]. However, the influence of sensory experience on synaptic plasticity in the hippocampus remains obscure. We assessed the effects of dark rearing in rats on short-term plasticity of excitatory synaptic connections and the dynamics of Aβ40 and Aβ42 isoforms in V1 and hippocampus (**Fig. 7**), starting at postnatal day (P) 8, before eye opening, until the end of the critical period (P35–42). As has been previously demonstrated[39], dark rearing did not alter short-term synaptic plasticity in excitatory synaptic connections from layer 4 to layer 2/3 visual cortex in P35–42 rats (**Fig. 7a,d**). Accordingly, dark rearing did not affect dynamics of either the Aβ40 or Aβ42 isoform in V1 with different patterns of neuronal activity (**Fig. 7b–d**).

Notably, we found that visual deprivation led to enhanced synaptic facilitation in CA3–CA1 synapses, as compared with that in normally reared rats (**Fig. 7e,h**). These alterations in hippocampal synaptic dynamics were paralleled by changes in Aβ40 dynamics (**Fig. 7f,g**) similar to those induced by the pharmacological manipulations described above, leading to an increase in Aβ40/42 selectively during bursts in slices from dark-reared rats (**Fig. 7h**). That is, hippocampal synapses with stronger short-term synaptic facilitation in dark-reared rats showed Aβ40/42 with a higher dynamic range and susceptibility to burst inputs.

Correlation between Aβ40/42 and synaptic dynamics

Our data revealed that changes in Aβ40/42 were strongly correlated with short-term synaptic facilitation and were affected by factors modulating synaptic release. To extend this observation, we plotted the relationship between the dynamics (burst/single ratio) of Aβ isoforms and short-term synaptic plasticity (burst/single ratio of the mean charge transfer per action potential, Q_{fEPSP}) per individual animal, across various experimental conditions ($n = 70$ animals, **Fig. 8a,b**). Short-term synaptic plasticity in CA3–CA1 connections varied considerably among individuals and between groups with different histories of synaptic activation. However, it significantly correlated with Aβ40 dynamics among individual animals (**Fig. 8a**). In contrast, we observed no correlation between synaptic and Aβ42 dynamics (**Fig. 8b**). Consequently, synaptic plasticity strongly correlated with Aβ40/42 dynamics among individuals (**Fig. 8c**), such that synaptic facilitation in excitatory hippocampal synapses was strongly associated with Aβ40/42 augmentation during high-frequency discharges. Given a linear correlation between Q_{fEPSP} and the number of released synaptic vesicles, our data indicate that the Aβ40/42 ratio depends on the total number of released vesicles.

DISCUSSION

For several decades, scientists have searched for the mechanisms initiating synaptic and cognitive dysfunctions in Alzheimer's disease. Many FAD-linked mutations in presenilin and APP proteins that cause reduction in the Aβ40/42 ratio have been discovered[15–17], emphasizing the Aβ40/42 ratio in FAD pathogenesis. However, how Aβ40/42 dynamics is regulated by neural network activity and experience remains a central unresolved question, essential for understanding sporadic Alzheimer's disease initiation and progression. In this study, we found that spike bursts and release properties of synapses regulated the conformation of PS1 subunit of γ-secretase, determining the Aβ40/42 ratio. In contrast to the situation in the many FAD mutations triggering overproduction of the more pathogenic Aβ42 isoform, our data highlight Aβ40 as the key determinant of experience-dependent Aβ40/42 dynamics in hippocampal circuits.

Burst as a positive regulator of Aβ40/42 dynamics

Neurons have been proposed to encode information in two main firing modes: isolated spikes and high-frequency spike bursts[25].

The probability of spike bursts depends on the behavioral state in a cell type– and region-specific manner. For example, most (~85%) of the spikes in primary sensory cortices occur in isolation[40]. In contrast, in the CA1 region of the hippocampus, half of place cell spikes occur in short high-frequency bursts[41]. Spike bursts have been hypothesized to represent a functional unit of information, increasing the reliability of neuronal communication[25]. This hypothesis recently received experimental support from the demonstration that the hippocampus can rely solely on bursts during memory encoding[42].

Although neuronal and synaptic activity have been shown to positively regulate total extracellular Aβ[21,22], the specific roles of spike firing patterns in regulation of Aβ40/42 ratio remained unexplored. Our data revealed that increase in the mean rate of single spikes indeed elevated absolute Aβ40 and Aβ42, but did not affect the Aβ40/42 ratio. Notably, however, change in the temporal spiking pattern by means of a shift from single spikes to high-frequency (≥20 Hz) spike bursts boosted Aβ40/42 owing to preferential increase in the Aβ40 production. Given that Aβ40/42 was comparable between periods of spontaneous neuronal activity and those of stimulation by single spikes, higher Ca^{2+} generated by high-frequency spike bursts seems to be required for Aβ40/42 augmentation.

Is Aβ40/42 solely determined by the characteristics of neuronal input, or is it also affected by synaptic properties of the neuron? Our data point toward regulation of Aβ40/42 augmentation during bursts by the properties of the synaptic filter. Synaptic circuits with lower release probability and high synaptic facilitation, optimized for efficient burst transfer, show higher Aβ40/42 augmentation by bursts and thus broader Aβ40/42 dynamic range. Conversely, circuits with higher release probability and synaptic depression, optimized for the transfer of single spikes, are characterized by reduced Aβ40/42. Remarkably, changes in synaptic filter properties and the Aβ40/42 ratio co-varied after alterations in sensory experience. Notably, visual deprivation by means of dark rearing triggered concomitant enhancement of short-term synaptic facilitation and Aβ40/42 augmentation by bursts in hippocampus, but not in V1 cortex (**Fig. 7**), reinforcing the correlation between synaptic and Aβ40/42 dynamics across circuits with different synaptic release properties and history of activation (**Fig. 8**). Thus, spike bursts and synapse release properties, which are central to synaptic dynamics and memory encoding, represent the basic features determining Aβ40/42 ratio in neural circuits.

Bursts induce PS1 conformational changes to boost Aβ40/42

PS1 is a nine-transmembrane-domain protein that contains the catalytic site of γ-secretase[43]. Although the detailed molecular mechanism underlying the precision of APP cleavage by γ-secretase is not fully understood, alterations in the Aβ40/42 ratio have been tightly linked to conformational changes in PS1 and APP–PS1 interactions[28,29]. Catalytically active PS1 molecules have been proposed to exist in an equilibrium of two conformational states: closed (close proximity between the PS1 N terminus and a large cytoplasmic loop domain) and open. These correspond to a predominant cleavage of APP at Aβ42 and Aβ40 sites, respectively[29]. FAD PS1 mutations trigger PS1 conformational changes toward a closed conformation, corresponding to lower Aβ40/42 ratio[28,29]. A subset of Aβ42-lowering nonsteroidal anti-inflammatory drugs has an opposite effect, inducing a shift toward an open conformation[44].

To explore the physiological, activity-dependent mechanisms that regulate PS1 structure, we used a FRET reporter of PS1 conformation[28]. We found that PS1 conformation was differentially regulated by the temporal pattern of spikes in hippocampal neurons. Whereas single, low-frequency spikes were not able to alter the basal PS1 conformation, high-frequency spike bursts triggered a reduction in FRET, which may reflect a stabilized, open PS1 conformation corresponding to a higher Aβ40/42 ratio. Thus, total spike numbers may regulate absolute Aβ40 and Aβ42 through β-secretase activity[21] and/or dynamin-dependent APP endocytosis[23], whereas the temporal pattern of spikes may regulate PS1 conformation and, consequently, the Aβ quality.

Our conclusion that burst-induced changes in PS1 conformation and Aβ40/42 are linked to Ca^{2+}-dependent synaptic vesicle exocytosis is supported by the following evidence: (i) PS1 conformational changes by bursts were abolished in synapses lacking SNARE-dependent vesicle exocytosis; (ii) complete block of Ca^{2+} flux through presynaptic N- and P/Q-type VGCCs abolished PS1 conformational changes and Aβ40/42 augmentation by bursts; (iii) decrease in synaptic facilitation through elevation in the extracellular Ca^{2+}/Mg^{2+} ratio reduced the burst sensitivity of PS1 conformation and Aβ40/42 augmentation; (iv) chelation of residual Ca^{2+} by the slow calcium buffer EGTA-AM reduced synaptic facilitation, PS1 conformational changes and Aβ40/42 augmentation by bursts; and (v) Aβ40/42 strongly correlated with the total synaptic vesicle release across different experimental protocols.

Strong depolarization, high cytosolic Ca^{2+} and high rate of exocytosis are required for changes in PS1 conformation and the Aβ40/42 ratio. PS1 conformational changes occurred on a timescale of minutes (**Fig. 3h**), making direct regulation of PS1 by membrane voltage implausible. On the basis of the absolute requirement of synaptic vesicle exocytosis for PS1 conformational changes, insertion of the PS1 γ-secretase complex or/and APP from releasable endosomal and synaptic vesicles to the cytoplasmic membrane may underlie the observed PS1 structural modifications during bursts. Owing to the molecular complexity and dynamics of vesicle fusion and release reactions, further studies are required to determine the detailed molecular mechanism underlying stabilization of an open PS1 conformation by high-frequency spike bursts.

Implication for sporadic Alzheimer's disease

Aging is the highest risk factor for the common, late-onset sporadic Alzheimer's disease. Synapse loss in the aging hippocampus may trigger a compensatory increase in synaptic strength[45] and decrease in synaptic facilitation[46]. As based on the positive regulation of Aβ40/42 by synaptic dynamics identified in this study, experience-dependent decline in synaptic facilitation may stabilize a closed PS1 conformation and consequently reduce Aβ40/42 during periods of spike bursts. These changes may constitute the early events leading to the pathology in sporadic Alzheimer's disease (**Supplementary Fig. 10**). Given an inverse correlation between the Aβ40/42 ratio and amyloid formation[8–10], conversion of synapses toward high-pass filter mode may reduce amyloidogenic potential of the peptide. Therefore, high-frequency spike bursts may protect facilitatory synapses by boosting the Aβ40/42 ratio, representing a new strategy for therapeutic intervention.

Our findings suggest that Aβ40/42 dynamics emerge from inherent properties of neural circuits, providing a possible mechanism for the influence of everyday experience on Alzheimer's disease susceptibility and development in humans[47,48] and FAD mouse models[49,50]. Co-regulation of glutamate and Aβ40/42 dynamics by experience, revealed by this study, emphasizes that synaptic transfer function is critical in health and disease and offers conceptual insights into the etiology of sporadic Alzheimer's disease.

METHODS

Methods and any associated references are available in the online version of the paper.

Note: Supplementary information is available in the online version of the paper.

ACKNOWLEDGMENTS

We thank B. De Strooper for discussions, O. Berezovska (Harvard Medical School) for providing GFP-PS1-RFP cDNA, S. Frere for comments on the manuscript, Y. Amitai for suggestions on an early version of the manuscript and all laboratory members for discussions. This work was supported by European Research Council (281403), Legacy Heritage Biomedical Program of the Israel Science Foundation (1925/08), Alzheimer's Association (NIRG-10-172308) and Israel Science Foundation (993/08 and 170/08) grants to I.S. and EUROSPIN and SynSys Consortia (FP7-HEALTH-F2-2009-241498 and FP7-HEALTH-F2-2009-242167) grants to N.B. I.D. is grateful to the Center for Nanoscience and Nanotechnology of Tel Aviv University and Azrieli Foundation for the award of doctoral fellowships.

AUTHOR CONTRIBUTIONS

I.D. designed, performed, analyzed and interpreted biochemical and electrophysiological experiments. H.F. designed, performed, analyzed and interpreted FRET and FM experiments. H.M. and N.G. performed and analyzed whole-cell voltage-clamp recordings. Y.B. helped to conduct western blot experiments. N.L. and N.B. provided Munc13-1/2 double knockout mice and assisted with the interpretation of results. I.S. designed the study, interpreted the results and supervised the project. I.S., I.D. and H.F. wrote the manuscript.

COMPETING FINANCIAL INTERESTS

The authors declare no competing financial interests.

1. Haass, C. & Selkoe, D.J. Soluble protein oligomers in neurodegeneration: lessons from the Alzheimer's amyloid β-peptide. *Nat. Rev. Mol. Cell Biol.* **8**, 101–112 (2007).
2. Palop, J.J. & Mucke, L. Amyloid-β-induced neuronal dysfunction in Alzheimer's disease: from synapses toward neural networks. *Nat. Neurosci.* **13**, 812–818 (2010).
3. Haass, C. *et al.* Amyloid β-peptide is produced by cultured cells during normal metabolism. *Nature* **359**, 322–325 (1992).
4. Seubert, P. *et al.* Isolation and quantification of soluble Alzheimer's β-peptide from biological fluids. *Nature* **359**, 325–327 (1992).
5. Shoji, M. *et al.* Production of the Alzheimer amyloid β protein by normal proteolytic processing. *Science* **258**, 126–129 (1992).
6. De Strooper, B. & Annaert, W. Proteolytic processing and cell biological functions of the amyloid precursor protein. *J. Cell Sci.* **113**, 1857–1870 (2000).
7. Haass, C. Take five—BACE and the γ-secretase quartet conduct Alzheimer's amyloid β-peptide generation. *EMBO J.* **23**, 483–488 (2004).
8. Jarrett, J.T., Berger, E.P. & Lansbury, P.T. Jr. The carboxy terminus of the beta amyloid protein is critical for the seeding of amyloid formation: implications for the pathogenesis of Alzheimer's disease. *Biochemistry* **32**, 4693–4697 (1993).
9. Hasegawa, K., Yamaguchi, I., Omata, S., Gejyo, F. & Naiki, H. Interaction between Aβ(1–42) and Aβ(1–40) in Alzheimer's β-amyloid fibril formation *in vitro*. *Biochemistry* **38**, 15514–15521 (1999).
10. Kuperstein, I. *et al.* Neurotoxicity of Alzheimer's disease Aβ peptides is induced by small changes in the $Aβ_{42}$ to $Aβ_{40}$ ratio. *EMBO J.* **29**, 3408–3420 (2010).
11. Tanzi, R.E. & Bertram, L. Twenty years of the Alzheimer's disease amyloid hypothesis: a genetic perspective. *Cell* **120**, 545–555 (2005).
12. De Strooper, B. Loss-of-function presenilin mutations in Alzheimer disease. *EMBO Rep.* **8**, 141–146 (2007).
13. Wolfe, M.S. When loss is gain: reduced presenilin proteolytic function leads to increased Aβ42/Aβ40. *EMBO Rep.* **8**, 136–140 (2007).
14. Bertram, L., Lill, C.M. & Tanzi, R.E. The genetics of Alzheimer disease: back to the future. *Neuron* **68**, 270–281 (2010).
15. Suzuki, N. *et al.* An increased percentage of long amyloid β protein secreted by familial amyloid β protein precursor ($βAPP_{717}$) mutants. *Science* **264**, 1336–1340 (1994).
16. Duff, K. *et al.* Increased amyloid-β42(43) in brains of mice expressing mutant presenilin 1. *Nature* **383**, 710–713 (1996).
17. Scheuner, D. *et al.* Secreted amyloid β-protein similar to that in the senile plaques of Alzheimer's disease is increased *in vivo* by the presenilin 1 and 2 and APP mutations linked to familial Alzheimer's disease. *Nat. Med.* **2**, 864–870 (1996).
18. Bentahir, M. *et al.* Presenilin clinical mutations can affect γ-secretase activity by different mechanisms. *J. Neurochem.* **96**, 732–742 (2006).
19. De Strooper, B. & Annaert, W. Novel research horizons for presenilins and γ-secretases in cell biology and disease. *Annu. Rev. Cell Dev. Biol.* **26**, 235–260 (2010).
20. Brouwers, N., Sleegers, K. & Van Broeckhoven, C. Molecular genetics of Alzheimer's disease: an update. *Ann. Med.* **40**, 562–583 (2008).
21. Kamenetz, F. *et al.* APP processing and synaptic function. *Neuron* **37**, 925–937 (2003).
22. Cirrito, J.R. *et al.* Synaptic activity regulates interstitial fluid amyloid-β levels *in vivo*. *Neuron* **48**, 913–922 (2005).
23. Cirrito, J.R. *et al.* Endocytosis is required for synaptic activity-dependent release of amyloid-β *in vivo*. *Neuron* **58**, 42–51 (2008).
24. Buxbaum, J.D. *et al.* Alzheimer amyloid protein precursor in the rat hippocampus: transport and processing through the perforant path. *J. Neurosci.* **18**, 9629–9637 (1998).
25. Lisman, J.E. Bursts as a unit of neural information: making unreliable synapses reliable. *Trends Neurosci.* **20**, 38–43 (1997).
26. Abramov, E. *et al.* Amyloid-β as a positive endogenous regulator of release probability at hippocampal synapses. *Nat. Neurosci.* **12**, 1567–1576 (2009).
27. Wei, W. *et al.* Amyloid β from axons and dendrites reduces local spine number and plasticity. *Nat. Neurosci.* **13**, 190–196 (2010).
28. Uemura, K. *et al.* Allosteric modulation of PS1/γ-secretase conformation correlates with amyloid $β_{42/40}$ ratio. *PLoS ONE* **4**, e7893 (2009).
29. Berezovska, O. *et al.* Familial Alzheimer's disease presenilin 1 mutations cause alterations in the conformation of presenilin and interactions with amyloid precursor protein. *J. Neurosci.* **25**, 3009–3017 (2005).
30. Wolfe, M.S. *et al.* Two transmembrane aspartates in presenilin-1 required for presenilin endoproteolysis and γ-secretase activity. *Nature* **398**, 513–517 (1999).
31. Varoqueaux, F. *et al.* Total arrest of spontaneous and evoked synaptic transmission but normal synaptogenesis in the absence of Munc13-mediated vesicle priming. *Proc. Natl. Acad. Sci. USA* **99**, 9037–9042 (2002).
32. Murthy, V.N. & De Camilli, P. Cell biology of the presynaptic terminal. *Annu. Rev. Neurosci.* **26**, 701–728 (2003).
33. Newton, A.J., Kirchhausen, T. & Murthy, V.N. Inhibition of dynamin completely blocks compensatory synaptic vesicle endocytosis. *Proc. Natl. Acad. Sci. USA* **103**, 17955–17960 (2006).
34. Zucker, R.S. & Regehr, W.G. Short-term synaptic plasticity. *Annu. Rev. Physiol.* **64**, 355–405 (2002).
35. Debanne, D., Guerineau, N.C., Gahwiler, B.H. & Thompson, S.M. Paired-pulse facilitation and depression at unitary synapses in rat hippocampus: quantal fluctuation affects subsequent release. *J. Physiol. (Lond.)* **491**, 163–176 (1996).
36. Jankowsky, J.L. *et al.* Mutant presenilins specifically elevate the levels of the 42 residue β-amyloid peptide *in vivo*: evidence for augmentation of a 42-specific γ secretase. *Hum. Mol. Genet.* **13**, 159–170 (2004).
37. Hubel, D.H. & Wiesel, T.N. Receptive fields of cells in striate cortex of very young, visually inexperienced kittens. *J. Neurophysiol.* **26**, 994–1002 (1963).
38. Witter, M.P. *et al.* Cortico-hippocampal communication by way of parallel parahippocampal-subicular pathways. *Hippocampus* **10**, 398–410 (2000).
39. Philpot, B.D., Sekhar, A.K., Shouval, H.Z. & Bear, M.F. Visual experience and deprivation bidirectionally modify the composition and function of NMDA receptors in visual cortex. *Neuron* **29**, 157–169 (2001).
40. de Kock, C.P.J. & Sakmann, B. High frequency action potential bursts (<100 Hz) in L2/3 and L5B thick tufted neurons in anaesthetized and awake rat primary somatosensory cortex. *J. Physiol. (Lond.)* **586**, 3353–3364 (2008).
41. Harris, K.D., Hirase, H., Leinekugel, X., Henze, D.A. & Buzsáki, G. Temporal interaction between single spikes and complex spike bursts in hippocampal pyramidal cells. *Neuron* **32**, 141–149 (2001).
42. Xu, W. *et al.* Distinct neuronal coding schemes in memory revealed by selective erasure of fast synchronous synaptic transmission. *Neuron* **73**, 990–1001 (2012).
43. De Strooper, B., Iwatsubo, T. & Wolfe, M.S. Presenilins and γ-secretase: structure, function, and role in Alzheimer disease. *Cold Spring Harb. Perspect. Med.* **2**, a006304 (2012).
44. Lleó, A. *et al.* Nonsteroidal anti-inflammatory drugs lower Aβ42 and change presenilin 1 conformation. *Nat. Med.* **10**, 1065–1066 (2004).
45. Rosenzweig, E.S. & Barnes, C.A. Impact of aging on hippocampal function: plasticity, network dynamics, and cognition. *Prog. Neurobiol.* **69**, 143–179 (2003).
46. Deupree, D.L., Bradley, J. & Turner, D.A. Age-related alterations in potentiation in the CA1 region in F344 rats. *Neurobiol. Aging* **14**, 249–258 (1993).
47. Katzman, R. Education and the prevalence of dementia and Alzheimer's disease. *Neurology* **43**, 13–20 (1993).
48. Stern, Y. *et al.* Influence of education and occupation on the incidence of Alzheimer's disease. *J. Am. Med. Assoc.* **271**, 1004–1010 (1994).
49. Lazarov, O. *et al.* Environmental enrichment reduces Aβ levels and amyloid deposition in transgenic mice. *Cell* **120**, 701–713 (2005).
50. Herring, A. *et al.* Preventive and therapeutic types of environmental enrichment counteract beta amyloid pathology by different molecular mechanisms. *Neurobiol. Dis.* **42**, 530–538 (2011).

ONLINE METHODS

Slice preparation and treatment. All animal experiments were approved by the Tel Aviv University Committee for Animal Care. Wistar rats 1–2 months old, 3-month-old APPswe/PS1dE9 (ref. 36) and corresponding wild-type mice (B6C3F1/J background), *App*$^{-/-}$ (ref. 51) and corresponding wild-type mice (C57BL/6J background) were used (both female and male). All animals were kept in a normal light/dark cycle (12 h/12 h), three animals per cage. Coronal slices (400 μm) of hippocampus and primary visual cortex (V1) were prepared as described[26]. Slices were transferred to a submerged recovery chamber at room temperature (21–23 °C). containing oxygenated (95% O_2 and 5% CO_2) artificial cerebrospinal fluid (ACSF) for 1 h before the experiment. The ACSF contained, in mM, NaCl, 125; KCl, 2.5; $CaCl_2$, 1.2; $MgCl_2$, 1.2; $NaHCO_3$, 25; NaH_2PO_4, 1.25; glucose, 25. After 1 h of recovery, slices were transferred to a stimulation chamber inside a mini-incubator (32 °C, 95% O_2 and 5% CO_2) for 1 h electrical stimulation (four slices per 500 μl ACSF).

Hippocampal cell culture. Primary cultures of CA3–CA1 hippocampal neurons were prepared from newborn Wistar rats on postnatal days 0–2, as described[26]. For the Munc13-1/2 double knockout (*Unc13a*$^{-/-}$*Unc13b*$^{-/-}$) mice[31], hippocampal cultures were prepared from embryonic day 19. The experiments were performed in mature (15–28 days *in vitro*) cultures.

Electrical stimulations of slices and cultures. Two distinct stimulation protocols were used, preserving the mean rate constant (3,600 stimuli per hour): (1) Single, low-frequency stimulation: 3,600 stimuli at 1 Hz; (2) High-frequency spike bursts: 3,600 stimuli consisting of 720 bursts; each burst containing 5 spikes with an inter-spike interval (ISI) of 10 ms (**Figs. 2**–**5**) or 20 ms (**Figs. 6** and **7**) and inter-burst interval (IBI) of 5 s. In **Figure 1**, ISIs of 100, 50, 20 and 10 ms within the bursts were tested. Stimulations were done in the presence of 50 μM NMDAR and 20 μM AMPAR antagonists (**Figs. 1** and **3**–**5**) or in the presence of 50 μM NMDAR only (**Figs. 6** and **7**). Cultures were stimulated in the same medium they were maintained in before stimulation. After stimulation, ACSF was collected from stimulating chamber for extracellular Aβ measurements by ELISA.

Slice electrophysiology. Intracellular EPSC and extracellular fEPSP recordings were performed in a recording chamber on the stage of Olympus BX51WI microscope. fEPSPs were recorded using a glass pipette containing ACSF (1–2 MΩ). Whole-cell patch pipettes (2–3 MΩ) were used to record EPSCs under a −70 mV holding potential using the following intracellular solution (in mM): potassium gluconate, 120; KCl, 3; HEPES, 10; NaCl, 8; $CaCl_2$, 0.5; EGTA, 5; Mg-ATP, 2; and GTP, 0.3; pH adjusted to 7.25 with NaOH. Serial resistance was not compensated. For AMPAR-mediated EPSCs recordings, AP5 (50 μM) and gabazine (30 μM, Tocris) were added to the ACSF solution. fEPSPs recordings were done in the presence of AP5 (50 μM). Stimuli in the Schaffer collateral–commissural pathway evoked fEPSPs or EPSCs responses that were recorded from the CA1 stratum radiatum. For intracortical recordings, the stimulating electrode was placed in layer 4 and the recording electrode in layer 2/3 of the same column. Stimulations were delivered through a glass suction electrode (10–20 μm tip) filled with ACSF. As fEPSPs were stable during the stimulation period in the presence of AP5, electrophysiological recordings were performed after the stimulation period in the micro-incubator (**Figs. 6** and **7**). For the measurements of short-term plasticity, fEPSPs and EPSCs were induced by bursts containing 5 spikes, ISI = 20 ms, IBI = 5 s. The change in fEPSP/EPSC slope between spikes in the burst was measured as percentage from the first fEPSP/EPSC. The integral of the burst-evoked fEPSP/EPSC was divided by the number of spikes to calculate the charge transfer per spike (Q_{fEPSP} and Q_{EPSC}). Recordings were excluded if the V_m exceeded −60 mV and R_s exceeded 25 MΩ, or if any of these properties or the fEPSP amplitude changed by >10% during the course of the recording. Signals were recorded using a MultiClamp 700A/B amplifiers, digitized by DigiData1440A (Molecular Devices) at 10 kHz, and filtered at 2 kHz. fEPSPs and EPSCs were analyzed by pClamp10 software (Molecular Devices).

Aβ detection. Concentrations of rat Aβ40 and Aβ42 in ACSF were determined following stimulations by sandwich ELISA using highly sensitive kits, Wako, cat. nos. 294-62501 and 292-64501 for Aβ40 and Aβ42, respectively; BNT77 (Aβ11-28) was used as a capture antibody, BA27 as the antibody for the C terminal of Aβ40 and BC05 for the C terminal of Aβ42. Quantification of human Aβ40 and Aβ42 concentrations were also determined using two additional sets of human Aβ sandwich ELISA kits: Wako, cat. nos. 292-62301 and 298-62401, and Millipore EZBRAIN40 and EZBRAIN42 (**Supplementary Fig. 9**). All ELISA kit procedures were done according to the manufacturer's instructions. In cultures, the background Aβ in the medium measured before stimulation was subtracted from the Aβ values after the stimulation. In acute slices, the background Aβ was negligible (<3% of the signal) and was not subtracted from stimulation-evoked Aβ values.

For measurements of intracellular Aβ40 and Aβ42, samples were prepared by homogenizing the tissue in ten volumes of cold guanidine buffer (5 M guanidine in 50 mM Tris-HCl, pH 8). Homogenates were mixed overnight in 4 °C, followed by dilution with ten volumes of cold casein buffer (0.25% casein, 0.05% sodium azide, 20 μg/ml aprotinin, 5 mM EDTA, 10 μg/ml leupeptin in PBS, pH 8). Samples were centrifuged at 16,000*g* for 20 min at 4 °C. Supernatant were loaded on Wako ELISA kits according to manufacturer's instructions.

PS1 FRET imaging and analysis. The Cer-PS1-Cit construct containing Cerulean (Cer) at the PS1 N terminus (NT) and Citrine (Cit) inserted into the large cytosolic transmembrane domain 6–7 loop region between amino acids 351 and 352 was generated on the basis of GFP-PS1-RFP, which was kindly provided by O. Berezovska[28]. GFP was replaced by Cer using AgeI and XhoI and RFP was replaced by Cit using NotI. PS1-Cer was constructed by excising Cit with NotI. FRET imaging and analysis were carried as described[52,53] using a FV1000 spectral confocal microscope (Olympus). Cer was excited at 440 nm and fluorescence emission was measured between 460 and 500 nm. Cit was imaged at 515 nm (excitation) and 525–560 nm (emission). Photobleaching of Cit was carried out with the 515 nm laser line, at 2.3 mW laser output. Images were 512 × 512 pixels, with a pixel width of 92–110 nm. *z*-stacks were collected from 3–4 μm optical slices, at 0.6–0.8 μm steps. Donor dequenching due to the desensitized acceptor was measured from Cer emission before and after the acceptor photobleaching. FRET efficiency, *E*, was then calculated using the equation $E = 1-I_{DA}/I_D$, where I_{DA} is the peak of donor emission in the presence of the acceptor and I_D is the peak after acceptor photobleaching. Detection of Cer/Cit signals was done using custom-written scripts in MATLAB as described earlier[52,53]. For FRET experiments, all of the bursts consisted of five pulses with ISI = 10 ms and IBI = 5 s (**Figs. 3**–**5**).

Dark rearing. Wistar rats were randomly assigned to the dark rearing (DR) or to the control, normal rearing (NR) groups. DR rats were kept in complete darkness for 4–5 weeks, from P8 to P35–P42. A parallel NR group was placed in a normal light/dark cycle (12 h/12 h). P35–P42 coronal hippocampal and visual cortex slices from DR and NR rats were prepared.

Immunoblot analysis. At the end of each stimulation, hippocampal slices were homogenized and prepared for the detection of full-length APP, soluble APP and APP-C-terminal fragment (APP-CTF) by western blotting as described previously[8]. Soluble APP was probed using anti-APP 22C11 monoclonal antibody (Millipore, cat. no. MAB348; 1:2,000) followed by HRP-conjugated goat anti-mouse (Jackson ImmunoResearch, Cat. 115-035-146; 1:5,000). Full-length APP and APP-αCTF were detected using rabbit anti-APP-CTF antibody (Calbiochem, Merck KGaA, cat. no. 171610; 1:10,000) followed by goat anti-rabbit HRP conjugated secondary antibody (Jackson ImmunoResearch, Cat. 111-035-144; 1:5,000). After detection, blots were stripped with Restore Western Blot Stripping Buffer (Pierce, Thermo Scientific) and then re-probed with mouse anti-actin (Sigma, cat. no. A3853; 1:10,000) and HRP-conjugated goat anti-mouse (Jackson ImmunoResearch, cat. no. 115-035-146; 1:5,000) antibodies as a loading control protein. All proteins were visualized by SuperSignal West Pico Chemiluminescent (Pierce; Thermo Scientific). Densitometry was performed using ImageJ software, and each band was normalized to its actin signal.

Chemical reagents. DNQX, baclofen, CCPA, dynasore and gabazine were purchased from Tocris; AP5, BAPTA-AM, cadmium chloride and tetanus toxin were purchased from Sigma; tetrodotoxin, ω-conotoxin GVIA and ω-agatoxin IVA from Almone Labs, BACE1 inhibitor IV and L-685,458 from Calbiochem, EGTA-AM from Invitrogen.

Statistical analysis. Error bars shown in the figures represent s.e.m. For biochemical and electrophysiological experiments, *n* designates the number of animals.

doi:10.1038/nn.3376

For imaging experiments, *n* designates the number of boutons (each experimental condition was repeated at least in three different batches of cultures). One-way ANOVA analysis with *post hoc* Bonferroni's tests were used to compare several conditions ($^{*}P < 0.05$; $^{**}P < 0.01$; $^{***}P < 0.001$). Unpaired two-tailed *t*-tests were used for two-group comparison. The nonparametric Spearman test was used for correlation analysis.

51. Zheng, H. *et al.* β-Amyloid precursor protein-deficient mice show reactive gliosis and decreased locomotor activity. *Cell* **81**, 525–531 (1995).
52. Laviv, T. *et al.* Basal GABA regulates $GABA_BR$ conformation and release probability at single hippocampal synapses. *Neuron* **67**, 253–267 (2010).
53. Laviv, T. *et al.* Compartmentalization of the GABAB receptor signaling complex is required for presynaptic inhibition at hippocampal synapses. *J. Neurosci.* **31**, 12523–12532 (2011).